E-ISSN: 2664-8784
P-ISSN: 2664-8776
IJRE 2025; 7(1): 11-25

www.engineeringpaper.net
Received: 15-11-2024
Accepted: 21-12-2024

Ashour Abdulsada Kazem
Senior Chief Engineer, Oil Pipelines Company, Iraq

Correspondence
Ashour Abdulsada Kazem
Senior Chief Engineer, Oil Pipelines Company, Iraq

Comprehensive microstructural and mechanical evaluation of tig welded joints between API 5L Gr.B carbon steel and ASTM A312 stainless steel using ER 309L and ER NiCrMo-3 electrodes

Ashour Abdulsada Kazem

DOI: https://doi.org/10.33545/26648776.2025.v7.i1a.69

Abstract
High-temperature applications require stainless steel as an essential material because its chromium and nickel content makes it show exceptional oxidation resistance. API 5L steels function as high-strength low-alloy steels that constitute critical components within oil and gas pipelines because of their strong mechanical features. The research focuses on examining the TIG welded interface between API 5L Gr-B steel and ASTM 312 stainless steel when using ER 309L and ER NiCrMo-3 filler metals as the welding technique. Displacements in the welded joints received comprehensive evaluation through optical microscopy combined with tensile testing and hardness testing and bending analysis. The microstructural analysis of weld metal made with ER 309L filler metal showed ferrite as the matrix with embedded acicular ferrite and delta ferrite islands in austenite austenitic structure. The weld metal that used ER NiCrMo-3 filler metal contained large nickel grains alongside insoluble precipitates within its nickel-based solid solution. The measurements revealed that the weld zone area became harder in comparison to the base metal material in both testing conditions. The weld metal made with ER 309L exhibited a hardness level of 263 Vickers yet the weld metal made with ER NiCrMo-3 reached 206 Vickers. The Bending tests on welded samples with ER NiCrMo-3 metal filler material showed cracks in the weld area which implied reduced ductility. The ER NiCrMo-3 stainless steel filled metal caused fractures to appear in the stainless steel section but ER 309L stainless steel filled metal caused fractures in the carbon steel section during tensile testing. The tests showed that welded joint ultimate tensile strength reached 550 MPa in ER NiCrMo-3 specimens while reaching 453 MPa in ER 309L specimens.

Keywords: API 5L pipes, stainless steel welding, non-homogeneous welding, ER 309L, ER NiCrMo-3, TIG welding, mechanical properties

Introduction
Industrial manufacturing requires welding as an essential technique which supports numerous sectors in their operational activities. Multiple elements deciding the suitable welding method include the materials used for joining and base metal thickness and electrical current selection. It is crucial to shield welded metal areas from atmosphere contact mainly because metals tend to swiftly oxidize during the molten state. GTAW welding requires protective inert shielding gases such as argon helium and nitrogen to create high-quality welds because these gases stop oxidation from occurring. GTAW stands as a popular stainless steel welding technique because it delivers reliable and precise results specifically on austenitic and ferritic stainless steel materials. The welding procedure leads to major microstructural modifications at the weld zone that create damaging effects on both the strength features and corrosion performance of the manufactured product. The successful welding results in GTAW depend on adequate weld pool protection as this measure stops harmful effects on welded joint integrity [1]. GTAW functions optimally for welding thin to medium thickness sheets which measure between 3 to 10 mm due to its capacity to generate high-quality metallurgical structure and required mechanical properties. The high-quality welds produced by GTAW enable it to work on a wide range of metal structures. GTAW cannot provide optimal economic value when utilized to join materials thicker than 10 mm because it works at a slow speed and produces limited metal buildup while sustaining shallow penetration [2].

HSLA steels find high usage in pipeline structures as part of their extensive application [3]. Available at a critical scale are pipelines for delivering gases and liquids through extended routes between production centers and consumer destinations. Underground pipelines hide most of their structure yet pipes, valves and pump stations along with compressors and terminals remain visible above the ground [4]. The 300 series austenitic stainless steels stand out as the most preferred steel types because they offer superior corrosion resistance and weldability alongside excellent machinability together with solid mechanical strength. Their excellent qualities extend across a wide spectrum of applications that include automotive use and domestic appliance requirements. Their minimal carbon ratio stops intergranular corrosion from developing. The microstructure of this metal type features carbide precipitation and sigma phase formation which produces hot cracking and a considerable decrease in mechanical properties near the heat-affected zone (HAZ) [5]. Welding different materials becomes more complicated because base metals display varied expansion rates and different plastic behavior characteristics and show microstructural incompatibilities. The welded joint experiences thermal and plastic strain mismatch based on joint geometry together with plate thickness which creates conditions for grain boundary brittle fractures and crack propagation [6]. Manufacturers perform welding of dissimilar metals even though it presents major difficulties because numerous industrial materials need joint operation when adjacent. The joining of low-alloy steels with austenitic stainless steels finds widespread use in the oil, gas, petrochemical, refinery and power generation industries. The combination of low-alloy steel affordability with austenitic stainless steel corrosion resistance has made this welding practice standard. The construction industry extensively uses API-grade low-alloy steels because these materials offer superior weldability together with mechanical strength and affordable prices [7, 8]. The application of low-alloy steels occurs mainly in cold temperature areas but stainless steel heat-resistant alloys remain the preferred choice when facing elevated temperatures. Austenitic stainless steel pipes function as power plant transportation systems for high-temperature steam. When operational parameters permit, industries decide to use carbon or low-alloy steels instead of stainless steel as they strive to lower expenses [9]. The study explores the combination of the TIG welding procedure and its application to fuse API 5L Gr-B steel with ASTM 312 stainless steel through utilization of ER 309L and ER NiCrMo-3 filler metals under non-homogenous conditions. The next section delivers extensive information about TIG welding procedures as well as essential welding parameters that determine weld quality outcomes. This review examines welding characteristics between API 5L Gr-B steel and ASTM 312 stainless steel and high-strength low-alloy steels with special focus on different types of stainless steels [10].

Fig 1: API 5L Carbon Steel Pipes and Stainless Steel Pipes Used in Industrial Applications

Related study: GTAW and TIG share a similar wiring process which produces the arc by utilizing a non-consumable tungsten electrode. The proper welding conditions prevent the tungsten electrode from melting. The combination of tungsten electrode and workpiece produces an electric arc which forms [11].

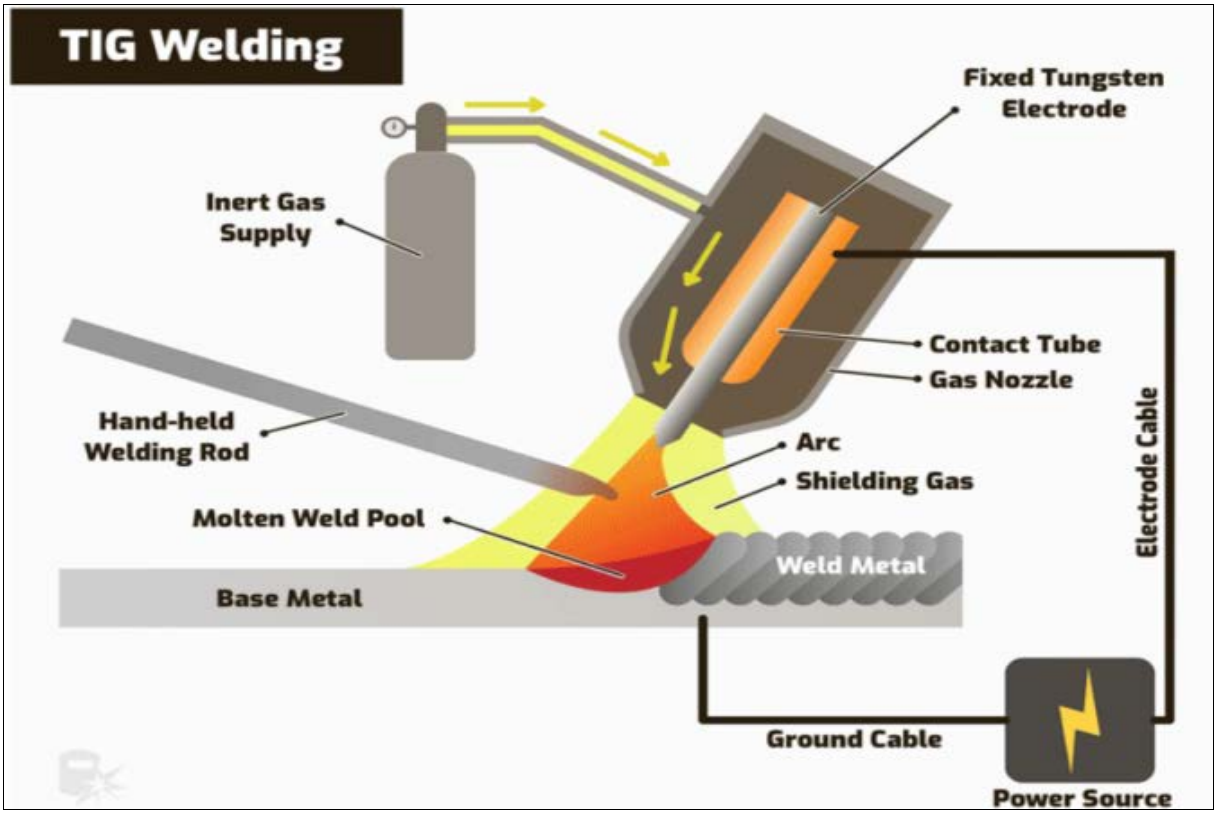

Fig 2: Schematic Diagram of TIG Welding Process

Filler Metals and Austenitic Stainless Steels

- Molten filler metals are specialized for thicknesses over 2mm and possess a chemical makeup similar to base materials.
- Automatic systems receive filler metals that come from rolls or coils with diameters between 1/6 to 3/2 millimeters.
- Welding of Austenitic stainless steels needs filler metals while additional heat treatment facilitates their joining process.
- The composition of filler metals in the 300 series includes modifications to stop hot cracking formation during solidification.
- The content of chromium in stainless steels surpasses iron to make them iron-based alloys designed with chromium as their main component.
- Stainless steel properties become stronger when nickel and molybdenum elements are added into their composition.
- The moisture corrosion resistance levels of stainless steel remain high in multiple operational settings.
- The material finds practical usage in pipeline systems and transportation devices and residential equipment systems.
- Ambient temperatures determine stainless steel microstructures into four distinctive groups.
- Martensitic stainless steels (with martensite microstructure)
- Ferritic stainless steels (with ferrite microstructure)
- Austenitic stainless steels (with ferrite microstructure)
- Austenitic-ferritic stainless steels contain both ferrite and austenite microstructure
- The special composition in HSLA steels achieves superior mechanical properties.
- The steel composition includes minimal amounts of niobium and titanium alongside vanadium for both structural hardness and structural fineness.
- Such stainless steels contain carbon at a maximum of 0.2% while the sum of all alloy elements remains under 2%.
- The elements niobium along with vanadium and titanium function as strong carbide and nitriding elements.
- Rising welding temperatures cause the disintegration of carbide and nitride entities thus reducing their protective capacity that stops grain enlargement.
- Heating large surface areas results in decreased toughness in those regions.
- Welding operations for HSLA steels should occur in their rolled or normalized condition.
- The majority of HSLA steels possess weldability properties that comparable to the weldability properties of mild steels.
- The production of big diameter welded pipes for petrochemical transmission lines uses API steel sheet material from the HSLA steel sheet family [12].

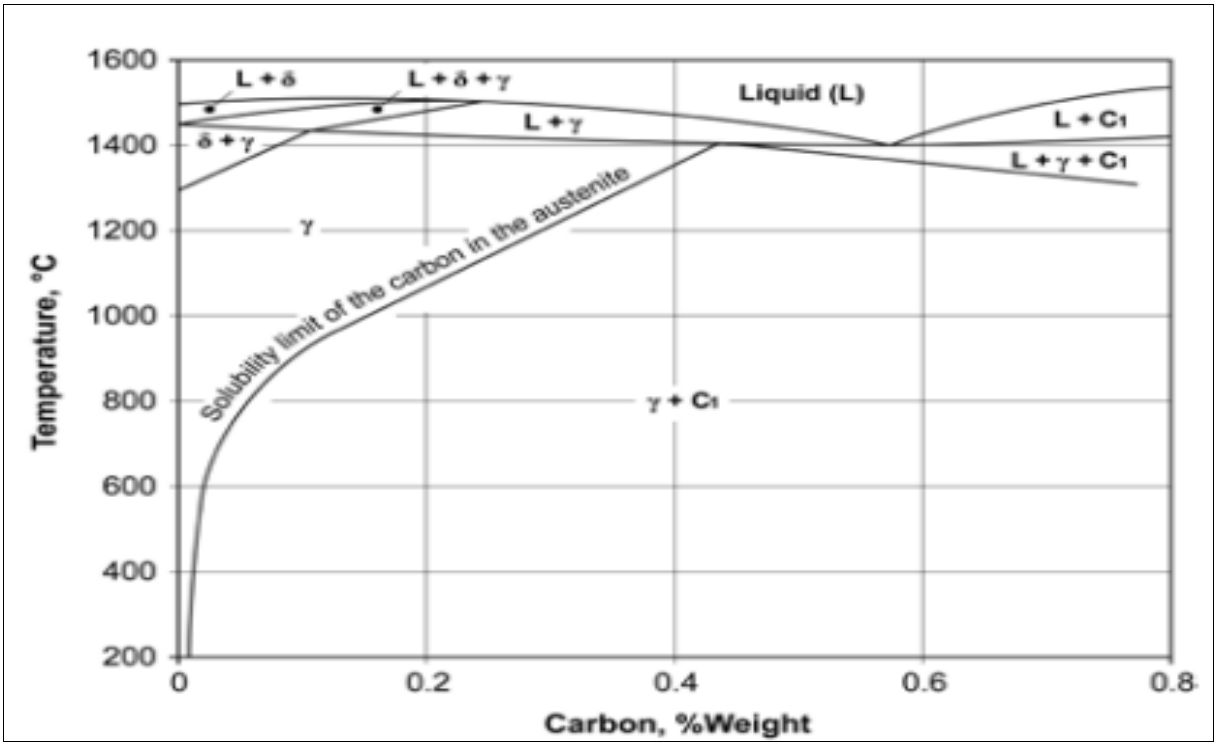

Fig 3: "Iron-Carbon Phase Diagram (Partial) Showing Austenite Solubility Limit"

2.2 Chemical Composition and Mechanical Properties of API 5L Grade B: In applications that need a moderate amount of pressure, the API 5L Grade B pipe material is a carbon steel pipe that is widely used for the transportation of water, natural gas, and petroleum under conditions of moderate pressure [12]. The fact that it has a chemical composition that is made of a maximum of 0.26% carbon, 1.20% manganese, and low levels of phosphorus and sulphur ensures that it is both weldable and resistant thanks to its makeup [13]. With a minimum yield strength of 245 MPa and a tensile strength of 415 MPa, it offers a balance of strength and ductility, as shown by the fact that it has both of these properties [14]. With a mild hardness of less than or equal to 200 HBW and an impact toughness of at least 27 J at a temperature of -30°C, this material is suitable for a wide range of applications, including those that include pipelines and structures [15]. When it comes to the oil, gas, and water extraction industries, API 5L Grade B continues to be a versatile and cost-effective solution. This is despite the fact that it is not as strong as grades from the X-series [16, 17].

Table 1: API 5L Grade B Mechanical and Chemical Properties

Property	Value
Yield Strength (MPa)	241.0
Tensile Strength (MPa)	414.0
Sulfur (S) Max	0.03
Phosphorus (P) Max	0.03
Manganese (Mn) Max	1.2
Carbon (C) Max	0.26

S-N Curve: Fatigue Behavior of Materials

The GTAW dissimilar welding of Incoloy 825 to AISI 321 using Inconel 625, Incoloy 65 and ER 347 filler materials received investigation by Siyar *et al.* 2018 [18]. A detailed inspection of weld zone metallurgy examined phase transformations together with grain structure and alloy dispersion patterns because these elements control weld high-temperature behavior [19]. Research findings showed that the materials present in the weld metal have a direct impact on microstructure formation and solidification patterns of the finished product. The fast cooling of Inconel 625 weld material produced austenite structure while the freezing phases shifted from cellular toward dendritic characteristics. Welding modifications created specific alterations in the mechanical characteristics together with the crack resistance capabilities of the joined section. The Incoloy 65 weld metal contained austenitic elements and dendritic shapes although its dendrite lengths surpassed those found in Inconel 625 which negatively affected both strength and toughness measures. The examination of ER 347 weld metal revealed that austenite remained as the primary matrix structure combined with ferrite due to the requirement of uniting different metal types with adjusted stabilizing element patterns. The microstructural area of weld metal exhibited a distinct distribution of alloying elements that altered its fusion zone arrangements [20]. Welding processes in the center produced mixed austenitic-ferritic and ferritic-austenitic structures that dictate mechanical properties and thermal stability of the joint. Siyar *et al.* exhibited complete understanding about solidification mechanisms and phase transformation behaviors during GTAW processes through rigorous microscopic investigations. According to Siyar *et al.* research in materials science scientists must select appropriate filler metals to gain precise control over welded properties as well as enhanced mechanical performance and industrial degradation protection for important processing operations such as chemicals and marine applications and power plants. The research data provides welding engineers together with metallurgists with fresh possibilities to create better heterogenous weld strategies for contemporary engineering systems.

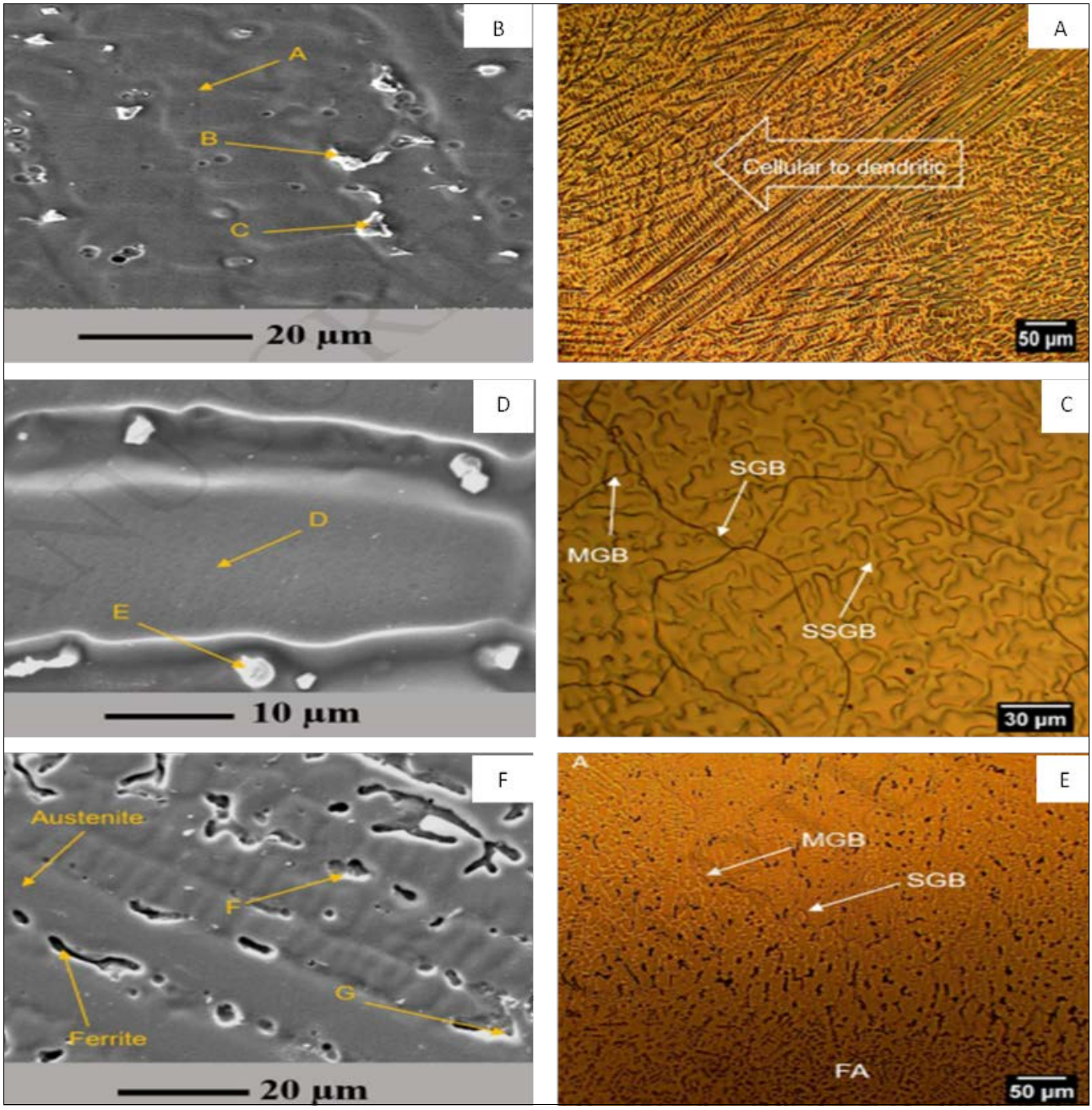

Fig 4: Microstructural Analysis of Welded Areas - Optical microscope and SEM images of different welding materials: (a, b) Inconel 625, (c, d) Incoloy 65, and (e, f) ER 347.

Effect of Filler Metals on AISI 321-Hastelloy C-22 Welded Joints

Sharma *et al.* 2019 [21] performed an extensive study that assessed how ERNiCrMo-4 and ERNiCrMo-3 filler metals affect the weld zone microstructure and mechanical performance as well as corrosion resistance of heterogeneous connections between AISI 321 stainless steel and Hastelloy C-22. A detailed analysis of weld zone transformations and material distribution patterns followed the research using modern microscopy as well as spectroscopy methods. The exploration of mechanical features which evaluated tensile strength together with hardness and impact resistance measured the structural strength of joints during different load requirements. Electrochemical tests assessed the weld corrosion resistance to determine how susceptible joints were to localized and uniform corrosion in destructive environments. The data demonstrates how filler metals selection brings important knowledge about durability enhancement and mechanical stability and corrosion resistance improvement of critical dissimilar metal welds used in aerospace and chemical engineering and power generation applications [21].

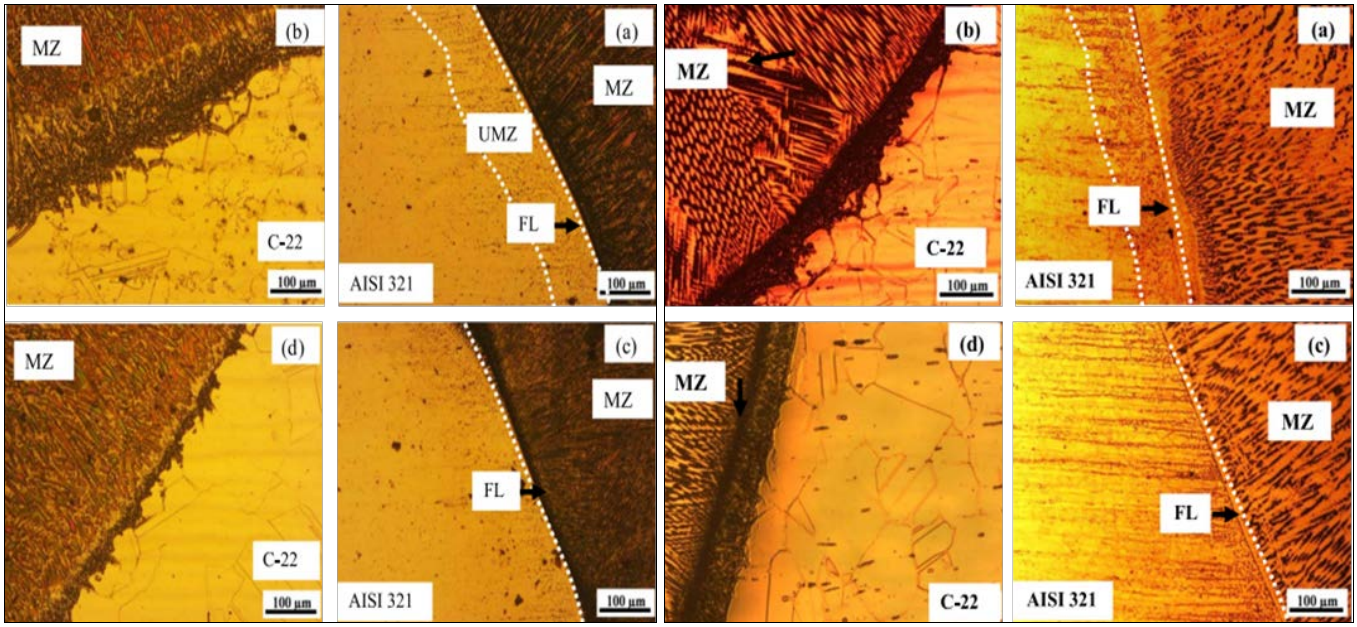

Fig 5: Optical Microstructures of Dissimilar Welds - Surface area microstructures of dissimilar welds using (a) ERNiCrMo-3 filler and (b) ERNiCrMo-4 filler, highlighting the differences in grain structure and weld morphology.

Effect of Filler Metals on API 5L X60 - AISI 310 Welds

Saedi *et al.* 2018 [22] studied the weldability and mechanical properties along with microstructural changes of API 5L X60 steel as it was joined to AISI 310 stainless steel by using ERNiCr-3, ER 310, ER 2209 and ER 309 filler metals. The two-phase ferrite-austenite boundaries in ER 2209 filler metal resulted in impact toughness of 91 J which proved to be the most pronounced among all studied materials. The optical microscopic analysis revealed that ER 310 weld metal contained stable austenitic cells and dendrites yet ER 2209 exhibited two-phase ferrite and austenite microstructurerones with no signs of intermetallic phases or carbide precipitation that boosted its mechanical performance. The impact toughness of ER 309 weld metal presented itself as moderate because it contained an austenitic matrix structure with delta ferrite forming skeletal patterns inside solidification cells. According to the study results ER 2209 stands out as the best filler metal because it achieves the optimal microstructural balance yet ER 310 offers improved stability in austenitic systems which makes them excellent choices for dissimilar metal welding applications [22].

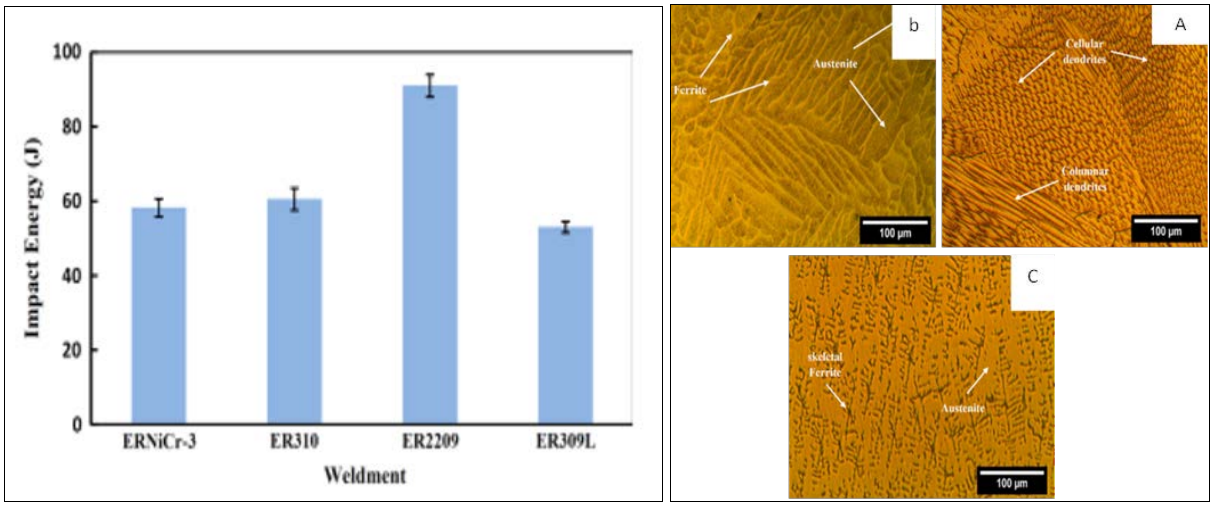

Fig 6: The figure compares the impact energy and microstructures of weldments using ERNiCr-3, ER 310, ER 2209, and ER 309L filler metals. ER 2209 exhibits the highest impact toughness, while microstructural analysis shows (A) ER 310 with cellular and columnar dendrites, (B) ER 2209 with a ferrite-austenite two-phase structure, and (C) ER 309L with skeletal ferrite in an austenitic matrix.

Microstructural Analysis of Weld Metal in P91 Steel

The steel material mainly contains blades of untempered martensite throughout austenite crystals. The heat produced by welding leads to the elimination of large precipitates without affecting refined precipitates that persist in the material [23]. The phase composition of weld metal depends on chromium and nickel equivalents that use elements to form austenite and ferrite. A fully martensitic microstructure forms when chromium equivalent values remain below 5.13 along with the condition of having Cr-Ni equivalent differences under 8. Analysis results indicate that the P91 weld metal contains a fully martensitic structure because its chromium equivalent measures 2.12 and Cr-Ni difference stands at 7.6. Weld metals consisting of chromium equivalents below 10 show no δ-ferrite formation since they lack ferritic structures according to research from P91 welds [24].

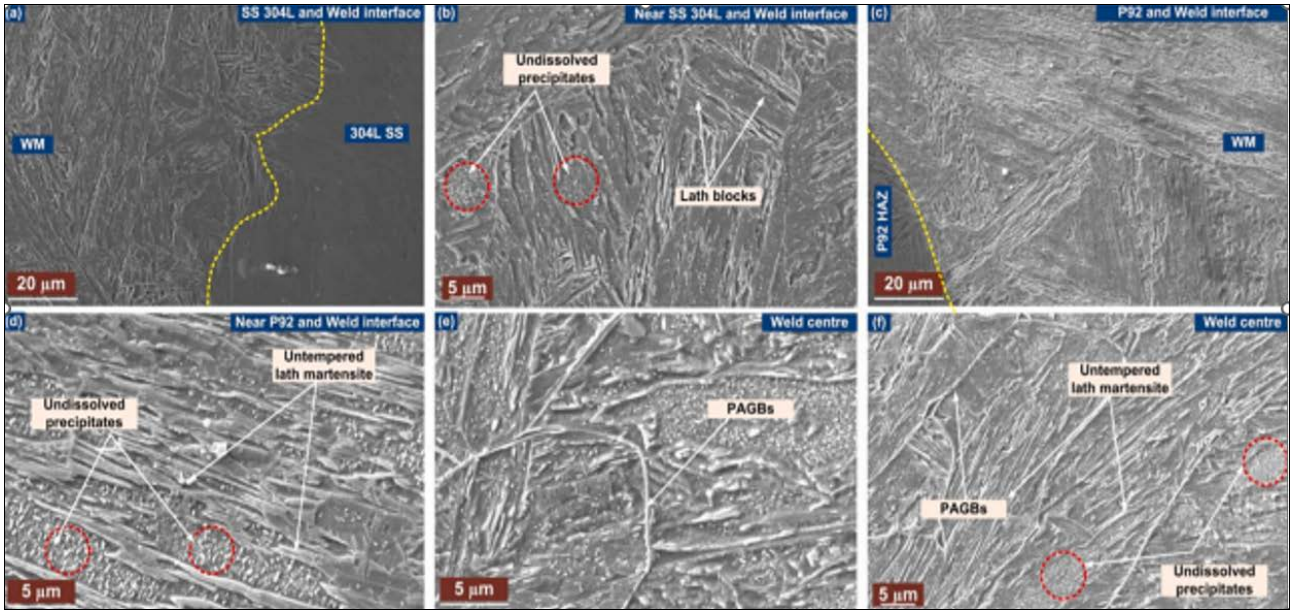

Fig 7: The location of microhardness measurement for the welding area and for both base metals is according to the figure. The dissolution of M23C6 sediments and some other sediments has increased the weight percentage of carbon and nitrogen in the CGHAZ area and has caused an increase in hardness in this area. The microhardness of the FGHAZ zone is reduced compared to the CGHAZ zone, which is due to the dissolution of M23C6 deposits, so less carbon and nitrogen are created in this zone.

Materials & Method

Materials: Two types of non-homogeneous pipes (carbon steel pipe API 5L Gr.B and stainless steel ASTM A312) with an outer diameter of 6 inches and a wall thickness of 7.82 mm

Two types of filler metal ER 309L and ER NiCrMo-3

Fig 7: Comparison of Carbon Steel and Stainless Steel Specimens in a Machining Environment.

Table 1: Welding Parameters for Different Passes

Pass	Process	Position	Filler Metal	Dia (mm)	Current	Polarity	Amp.	Volt	Travel Speed (cm/min)
ROOT	GTAW	ALL	ER309L	2.4	DCSP	80-130	8-12	5-10	
HOT	GTAW	ALL	ER309L	2.4	DCSP	80-130	8-12	5-10	
FILL	SMAW	ALL	E309L	2.6	DCRP	60-110	18-28	4-10	
CAP	SMAW	ALL	E309L	2.6	DCRP	60-110	18-28	4-10	

Table 2: Welding Parameters Using NiCrMo-3 Filler Metal

Pass	Process	Position	Filler Metal	Dia (mm)	Current	Polarity	Amp.	Volt	Travel Speed (cm/min)
ROOT	GTAW	ALL	ER NiCrMo-3	2.4	DCSP	80-130	8-12	5-10	
HOT	GTAW	ALL	ER NiCrMo-3	2.4	DCSP	80-130	8-12	5-10	
FILL	SMAW	ALL	E NiCrMo-3	2.6	DCRP	60-110	18-28	4-10	
CAP	SMAW	ALL	E NiCrMo-3	2.6	DCRP	60-110	18-28	4-10	

Methods

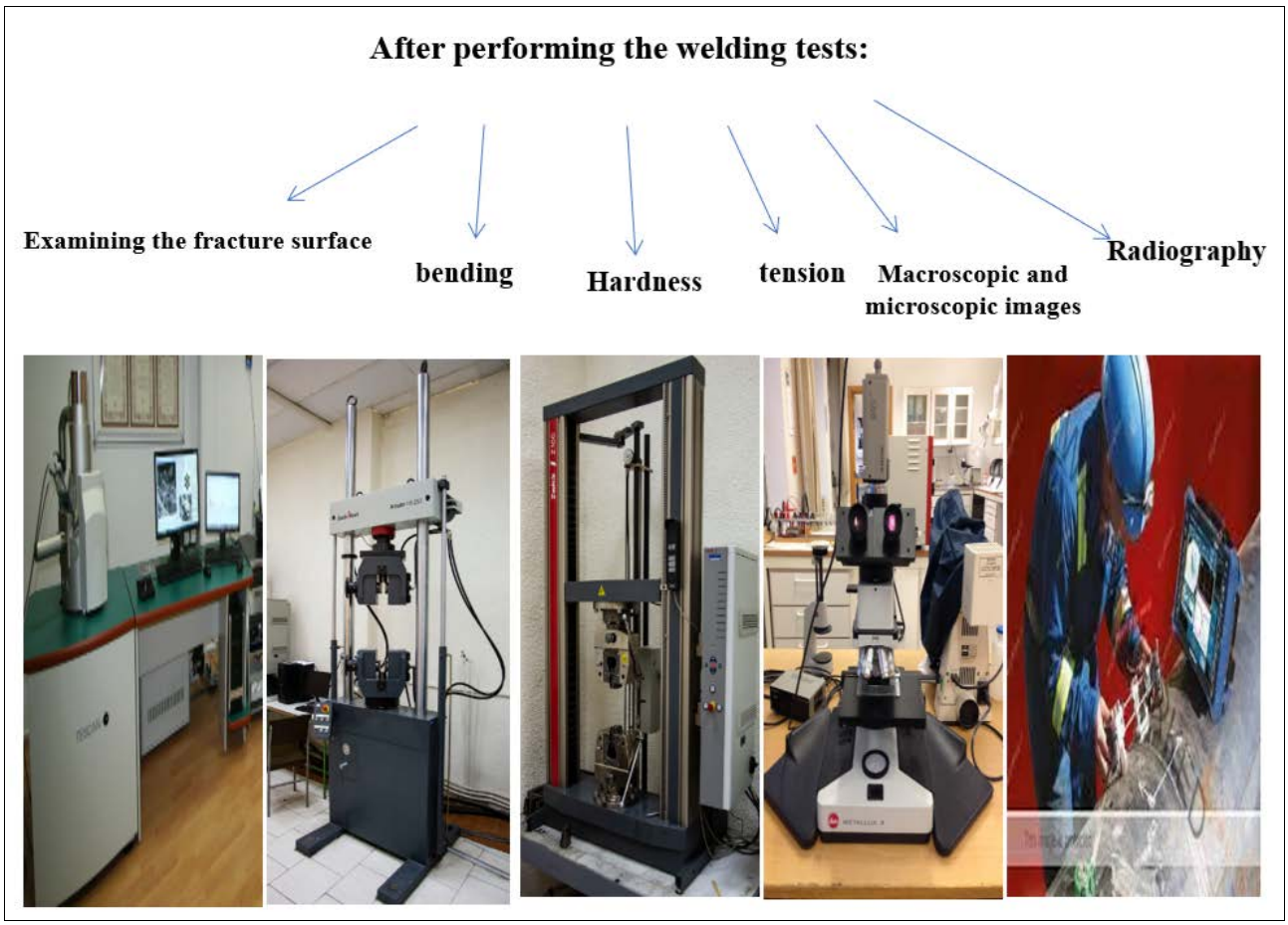

Results & Discussion

Radiographic test results

In the course of the welding procedure that makes use of ER NiCrMo-3 filler metal, it has been observed that there is a discontinuity in the joint area. According to the radiography images, the connection that was made from the ER309L filler metal is of a better grade than the one that was obtained from the ER NiCrMo-3 filler metal. This is something that may be seen by contrasting the two with one another.

Appearance quality of welded pipes

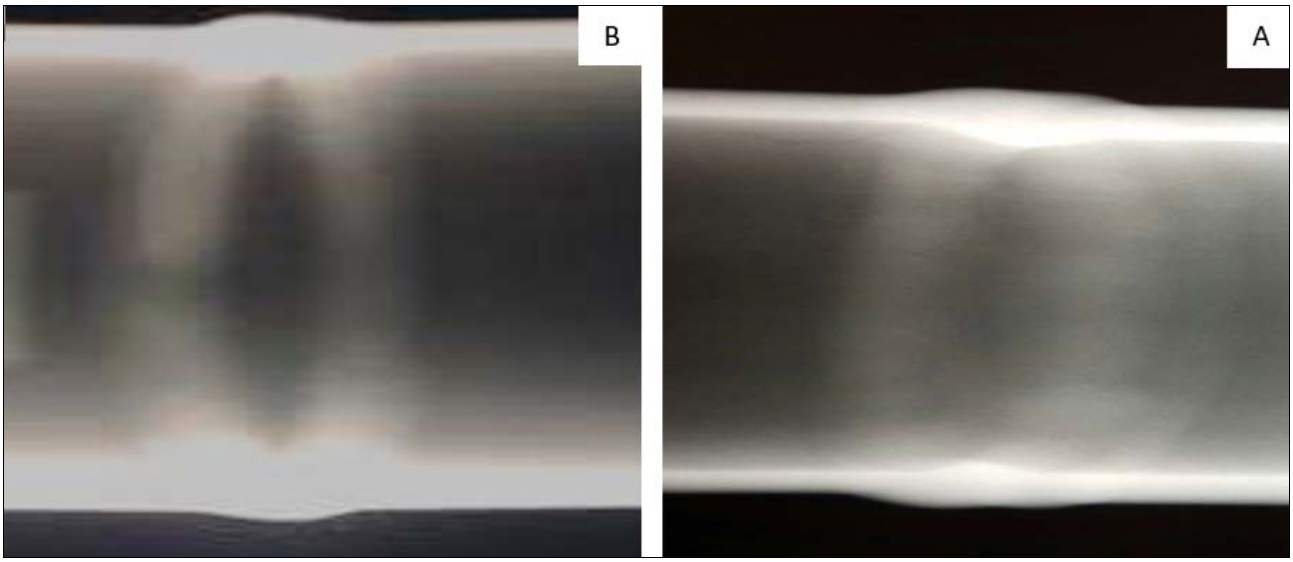

Fig 8: Radiographic Images of Femoral Bone Healing in the Control Group ((A) Shows the femoral bone with minimal bone regeneration at the defect site. (B) Displays delayed healing with low-density bone formation and a visible defect area).

Appearance quality of welded pipes

Fig 9: Welded Joint between Stainless Steel and Carbon Steel ((A) Close-up view of the welded joint between stainless steel (SS A312) and carbon steel (CS API 5L Gr. B), showing the weld seam and markings. (B) Full view of the welded specimen, highlighting material specifications and dimensions.

Macroscopic images using ER 309L filler metal

Macroscopic weld evaluation showed that the weld root contained no defects while final welds lacked both gas voids and slag implications. The weld bead height measurement processed the following figures: 2 mm at the 6 o'clock position and 2.3 mm at the 12 o'clock position. Laboratory testing proved that improper base metal to weld metal fusion did not take place since no incomplete melting deficiencies were identified. Weld penetration tests declared structural integrity because both base metal penetration measurements and inter-layer analysis met target specifications. The macroscopic examination using ER NiCrMo-3 filler metal demonstrated the weld root had complete fusion while showing no weld defects of cracks or sidewall undercuts or fractures. The measurements taken through ImageJ verified the weld pollen height at 2.3 mm precisely. A small porosity measuring 0.27 mm in diameter was discovered in the welded area according to the analysis that included a red arrow mark. The merged sections displayed outstanding quality though one tiny porosity existed within the welded area.

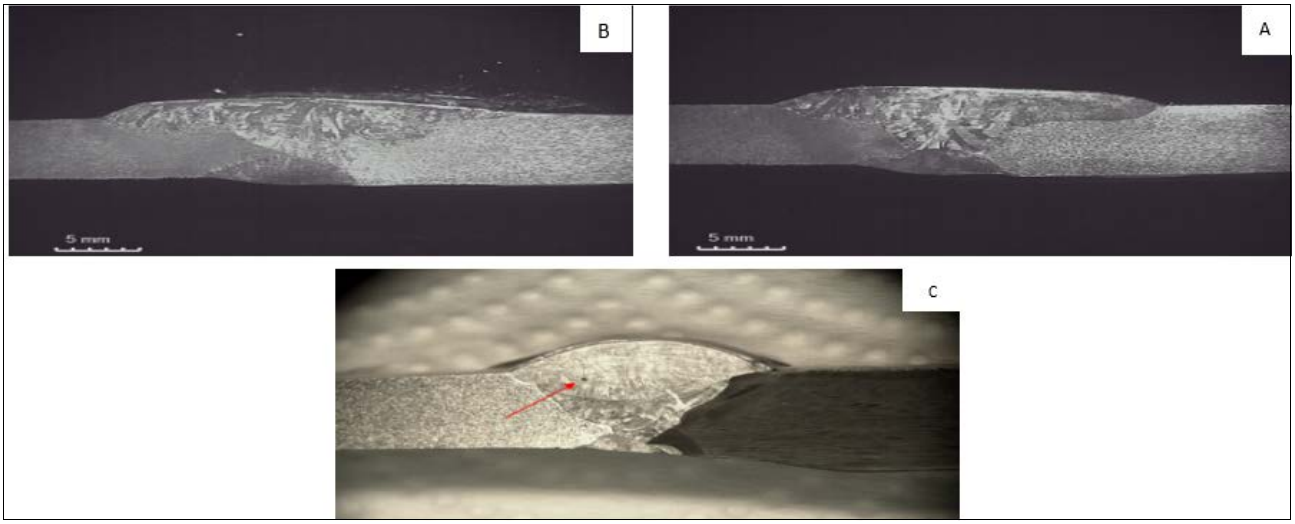

Fig 10: Macroscopic Examination of Welded Joints (Macroscopic images of the welded joints reveal uniform fusion and penetration in sections (A) and (B), demonstrating the integrity of the weld. In (C), a minor porosity defect is observed (indicated by the red arrow), highlighting a small imperfection within the weld structure).

Microstructural Analysis of API 5L Gr-B and ASTM Base Metals

Macroscopic weld evaluation showed that the weld root contained no defects while final welds lacked both gas voids and slag implications. The weld bead height measurement processed the following figures: 2 mm at the 6 o'clock position and 2.3 mm at the 12 o'clock position. Laboratory testing proved that improper base metal to weld metal fusion did not take place since no incomplete melting deficiencies were identified. Weld penetration tests declared structural integrity because both base metal penetration measurements and inter-layer analysis met target specifications. The macroscopic examination using ER NiCrMo-3 filler metal demonstrated the weld root had complete fusion while showing no weld defects of cracks or sidewall undercuts or fractures. The measurements taken through ImageJ verified the weld pollen height at 2.3 mm precisely. A small porosity measuring 0.27 mm in diameter was discovered in the welded area according to the analysis that included a red arrow mark. The merged sections displayed outstanding quality though one tiny porosity existed within the welded area.

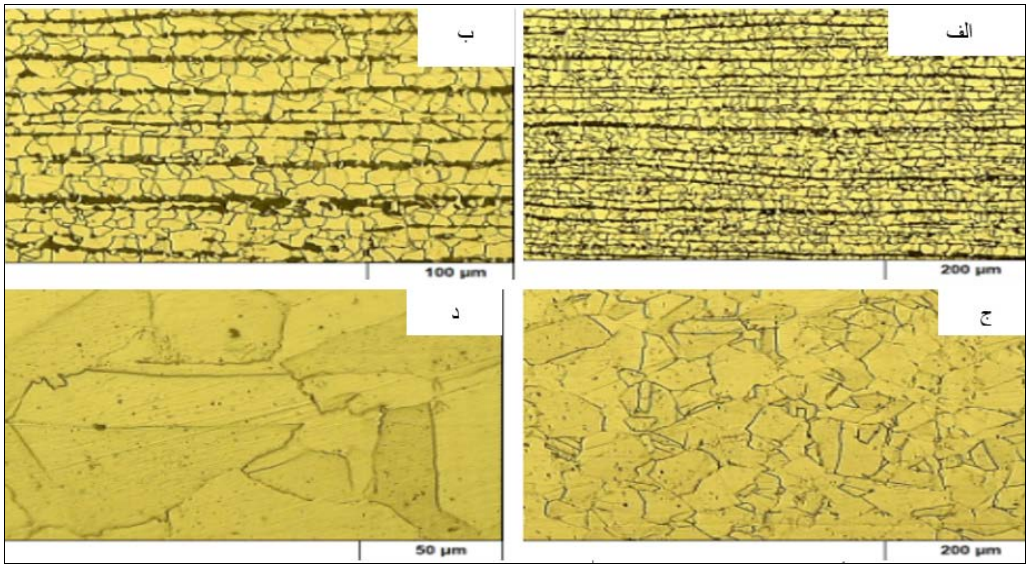

Fig 11: Microstructural Analysis of API 5L Gr-B and ASTM 312 Base Metals ((أ) Microstructure of ASTM 312 base metal, showing austenite grains with distinct twin bands. (ب) Microstructure of the weld metal, exhibiting a dendritic solidification structure. (ج) Heat-affected zone (HAZ) of API 5L Gr-B, revealing coarse-grained ferrite with pearlite regions. (د) Microstructure of API 5L Gr-B base metal, consisting of ferrite grains interspersed with aligned rows of pearlite).

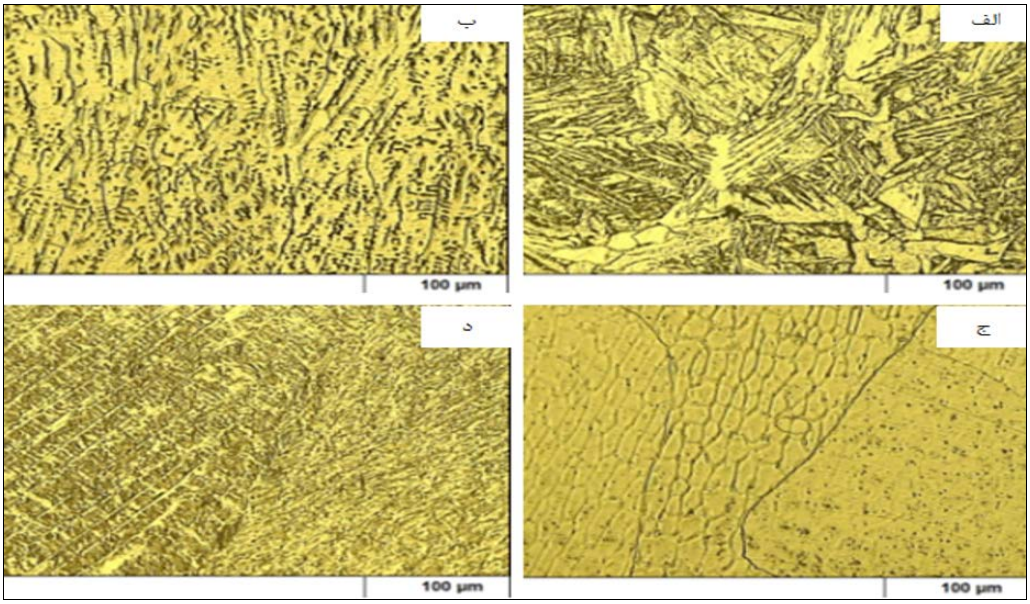

Fig 12: Microstructural Analysis of API 5L Gr-B and ASTM 312 Welded Joint (Micrographs illustrating different regions of the welded joint: (أ) Weld metal showing a lamellar structure, (ب) Heat-affected zone (HAZ) of ASTM 312 with austenite grains and deformation bands, (ج) API 5L Gr-B base metal with equiaxed ferrite and pearlite, and (د) ASTM 312 base metal featuring austenitic grains with distinct twin bands).

Hardness Distribution in Weld Metal and Heat-Affected Zones: The hardness of welded material exceeds both base materials and heat-affected zones in all filler metal series. The microstructural development of weld metals changes due to rapid cooling during welding but this leads to the formation of hard phases. Having achieved strength-enhancing microstructural transformations makes the weld metal perform better than adjacent zones because it creates superior mechanical stability along with increased resistance to wear. Studies on these two filler metals prove that weld metals made from ER 309L reach better average hardness levels than those welded with ER NiCrMo-3. Average hardness levels differentiate according to the chemical substance compositions found in filler metals. The stainless steel-based filler metal ER 309L forms high-quality mechanical properties due to its elevated chromium and nickel content. Weld metals created from ER 309L become harder because its key alloying elements result in permanent phase formation. The main purpose of employing ER NiCrMo-3 results in producing nickel-based metal that combines excellent corrosion resistance with high ductility and toughness for harsh conditions. ER NiCrMo-3 exhibits slightly greater hardness compared to ER 309L because the filler metals possess different chemical content. The stable ductile microstructure of ER 309L material makes its weld metal retain enhanced microstructure and achieve better hardness than ER NiCrMo-3 weld metal because it resists environmental damage for longer. The selection of suitable filler metal influences weld applications because it establishes a balance between hardness and ductility together with corrosion resistance to extend material lifetime.

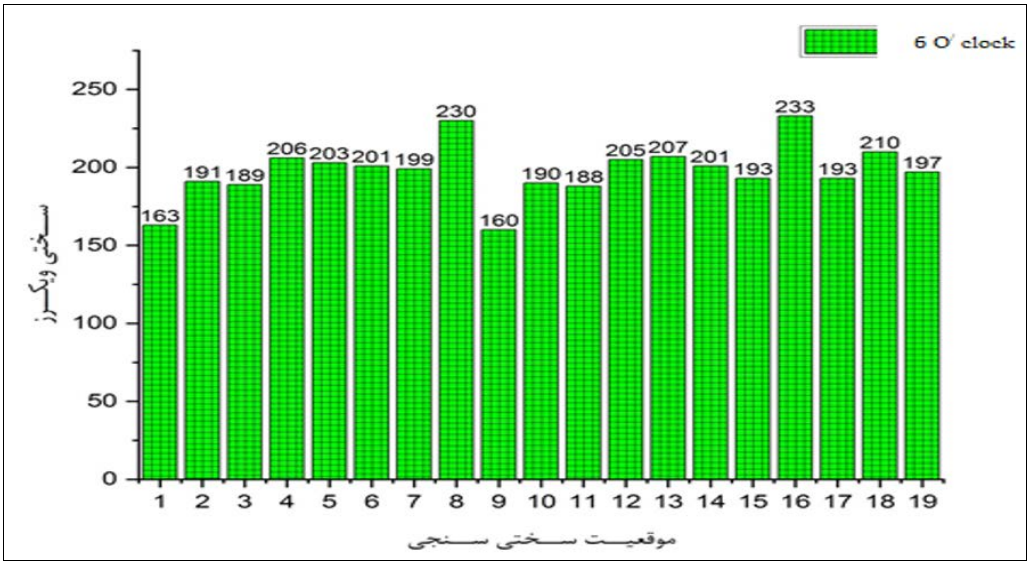

Fig 13: Vickers Hardness Distribution at the 6 O'clock Position (Bar graph showing the Vickers hardness values for a tube welded using ER NiCrMo-3 filler metal, highlighting variations in hardness across the weld metal, heat-affected zone (HAZ), and base metal.

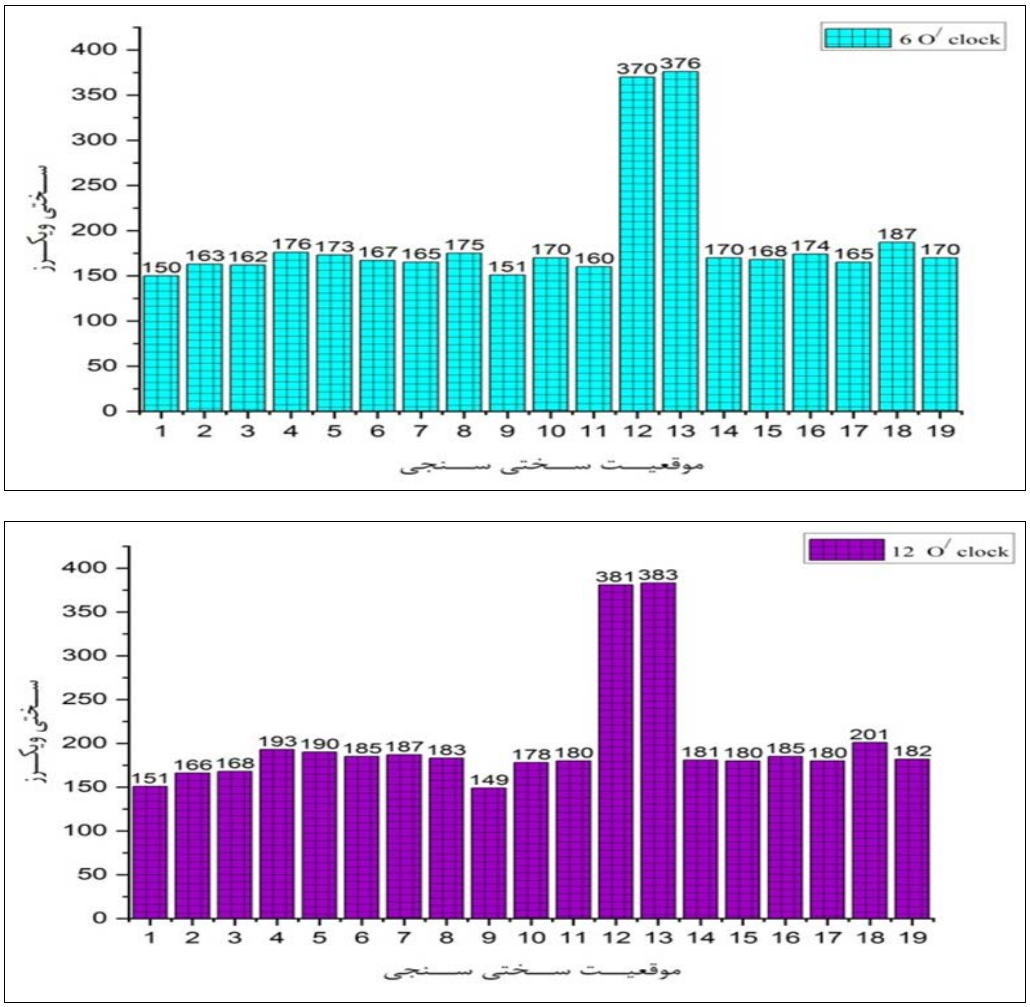

Fig 14: Vickers Hardness Distribution at 6 O'clock and 12 O'clock Positions for a Tube Welded with ER 309L Filler Metal (Bar graphs illustrating the Vickers hardness values at 6 o'clock (top) and 12 o'clock (bottom) positions along the welded tube using ER 309L filler metal. The hardness variations reflect differences in the microstructural properties across the weld metal, heat-affected zone (HAZ), and base metal).

Bending Test Results: The bending test showed distinct outcomes between the weld qualities of the two filler metals. The welds made with ER NiCrMo-3 filler metal showed the appearance of cracking at the root area of weld metal. The measured cracks from the bend test showed their maximum at 86.3 mm and their minimum at 0.8 mm which demonstrates failure risk under bending conditions. The welds made with ER 309L filler metal showed excellent mechanical qualities by keeping the bent samples entirely free of cracks or visible defects during the bending tests.

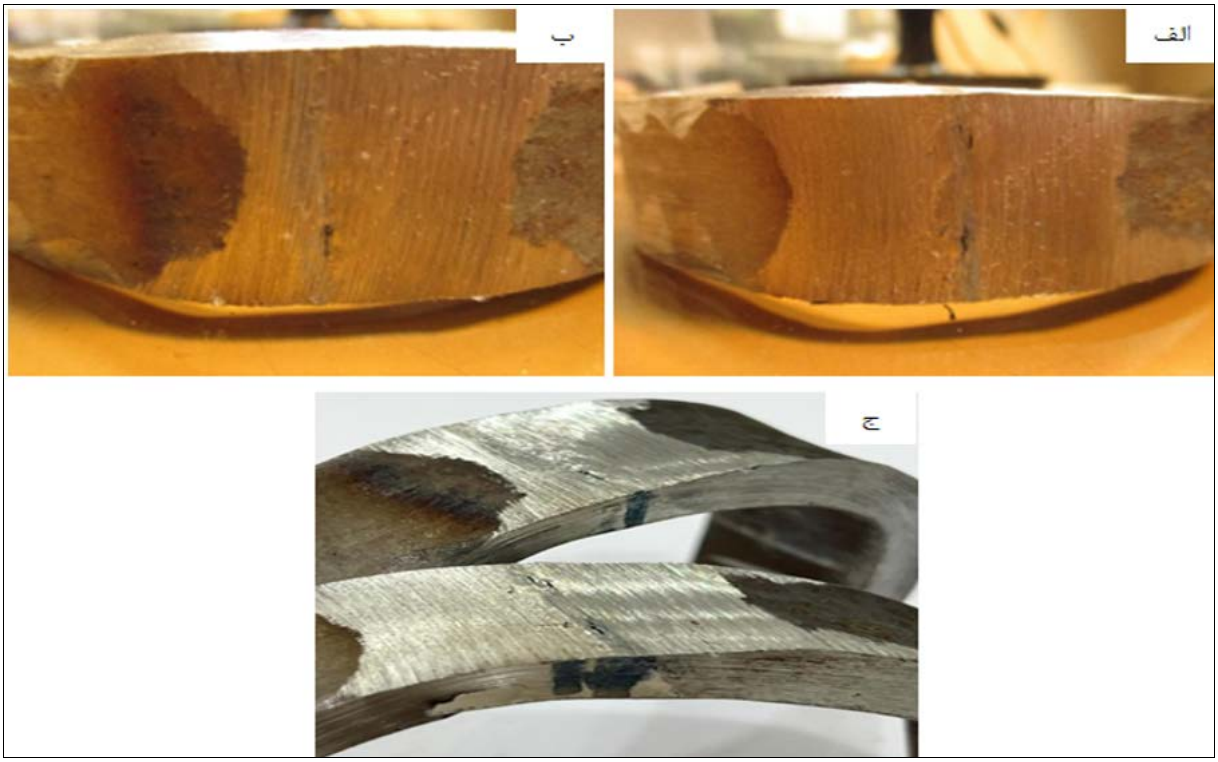

Fig 15: Bending Test Results for Welded Samples (Macroscopic examination of bent samples reveals cracks in the weld metal for ER NiCrMo-3 filler metal (أ,ب), originating from the root area, with varying crack lengths. In contrast, the sample welded with ER 309L filler metal (ج) remained free of cracks and defects, demonstrating superior mechanical integrity and resistance to bending deformation.

Tensile Properties of the Pipes Used in This Research

Table 4: Tensile and Yield Strength of the Pipes Used in This Research

Grade	Tensile Strength (min, MPa)	Yield Strength (min, MPa)
ASTM 312	485	170
API 5L Gr-B	415	240

Table 5: Tensile Test Results for Welded Samples with ER NiCrMo-3 Filler Metal

Specimen	Sampling Position	Dimension A*B (mm)	Initial Area (mm²)	Y.S (MPa)	U.T.S (MPa)
1	TT(1,2)	19.09×7.44	142.02	N.A	534
2	TT(7,8)	19.09×7.46	142.18	N.A	560
Location of Fracture	BM (A312 Grade 304) for both specimens				

Table 6: Tensile Test Results for the Sample Welded with ER 309L Filler Metal

Specimen	Sampling Position	Dimension A*B (mm)	Initial Area (mm²)	Y.S (MPa)	U.T.S (MPa)
1	TT(1,2)	19.38×7.39	143.21	N.A	448
2	TT(7,8)	19.28×7.32	141.12	N.A	458
Location of Fracture	BM (Carbon Steel) for both specimens				

Fractographic Analysis of Welded Samples Using scanning electron microscope SEM

The scanning electron microscope (SEM) acquired images to examine the fracture cross-sections obtained from both filler metals. These inspections detected the existence of voids because they indicate a delicate fracture process. Medical analysis revealed a ductile fracture of reduced depth in the tested specimen that received ER 309L filler metal welding. Research indicates the fracture location at the carbon steel zone where voids are deep although wide leading to a shorter pathway than previously predicted. A fracture occurred throughout the section of the stainless steel-filled area with ER NiCrMo-3 filler metal. A sudden soft failure occurred due to this event which produced numerous deeper voids that were also smaller in size. The fractography evaluation between ER NiCrMo-3 welds shows that void numbers steadily increase as the material depth extends below the surface. Expert findings about void formation stemmed from analyzing the photographs. The pre-failure plastic deformation has demonstrated substantial enhancement according to these results. The presented case reveals that deep voids indicate ductile failure behavior because it shows dissimilar fracture patterns between these two filler metals. These deep holes in the test material indicate ductile failure processes take place during the failure mechanism.

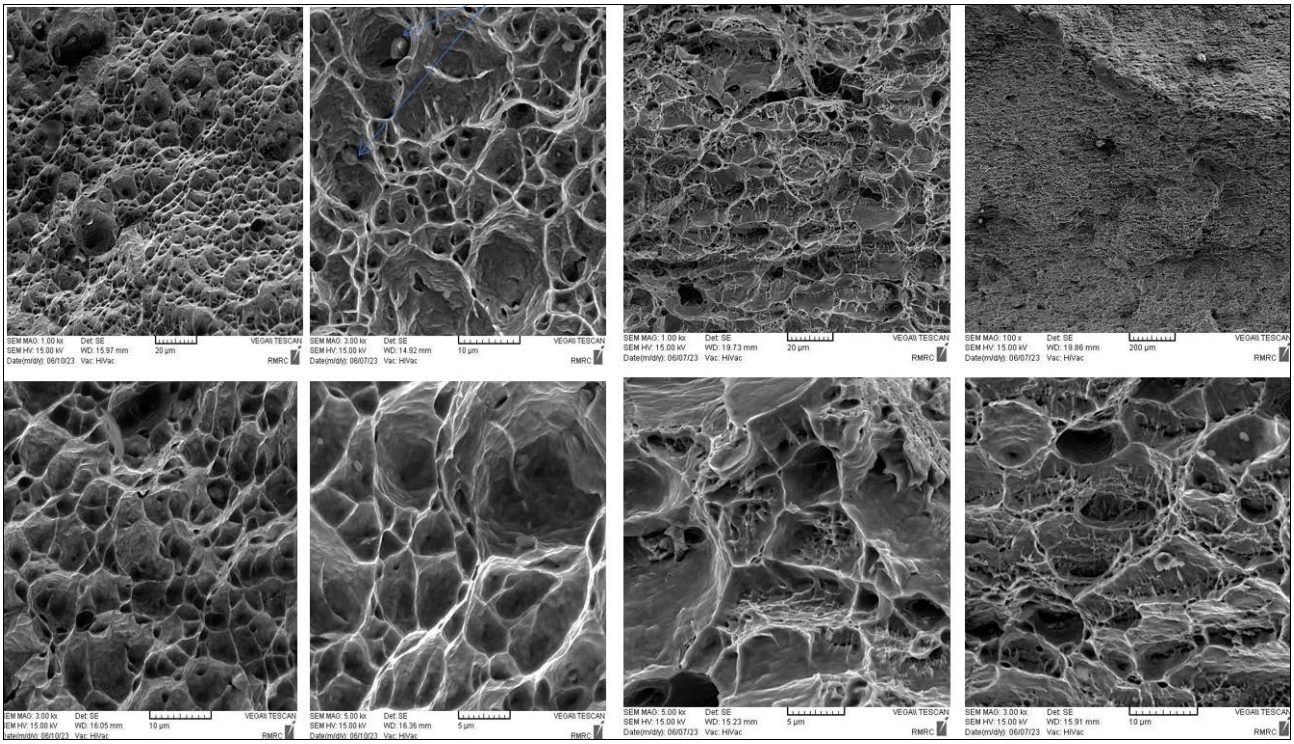

Fig 18 and 19: SEM Fractographic Analysis of Welded Samples Using ER 309L and ER NiCrMo-3 Filler Metals (These scanning electron microscope (SEM) images illustrate the fracture surfaces of welded samples. The fracture morphology in ER 309L welds (Figure 18) shows larger and shallower voids, indicating a ductile fracture in the carbon steel region. In contrast, the fracture surfaces in ER NiCrMo-3 welds (Figure 19) exhibit a higher density of finer and deeper voids, signifying a softer failure mode in the stainless steel region).

Discussion

A complete examination details the weld quality as well as the mechanical properties and fracture deficiencies of interfaces produced with ER 309L and ER NiCrMo-3 filler metals. The analysis consists of various tests that include radiographic inspections in addition to macroscopic and microstructural examinations and hardness measurements and bending and tensile tests and SEM-based fractographic investigations. These research results give essential understanding about how the filler metal composition affects weld strength and mechanical properties together with the failure patterns. The weld made with ER 309L created better fusion and produced less defective results than the ER NiCrMo-3 weld according to radiographic results [25]. Metallurgical bond strength increased through the elevated chromium and nickel content of ER 309L that produced a weld with superior quality. Macroscopic examination showed that the filler metals contained no signs of cracking and gas voids combined with no slag impurities. The weld deposits showed 2 mm height at the 6 o'clock orientation alongside 2.3 mm at the opposite 12 o'clock orientation indicating uniform layer distribution. A small porosity problem (0.27 mm) affected the durability potential of ER NiCrMo-3. Both welding processes resulted in complete penetration along with proper fusion because of the effective welding parameter choices. The microscopic investigation revealed substantial dissimilarities that existed between the initial metal components and their welded areas. Within the API 5L Gr-B part numerous ferrite-pearlite characteristics appeared alongside strength and wear resistance properties whereas ASTM 312 exhibited an austenitic structure containing twin bands which supported corrosion resistance and deformation toughness. The different microstructures developed between the weld metals affected their properties because ER 309L produced fine lamellae which improved hardness while ER NiCrMo-3 formed dendrites which enhanced ductility. Weld metal hardness exceeded the hardness of heat-affected zone (HAZ) and base metal components because rapid cooling triggered phase transformations. The weld strength of ER 309L exceeded ER NiCrMo-3 weld strength because its chromium and nickel content stabilized harder phases in the weld structure. ER NiCrMo-3 welds provide excellent ductility together with corrosion resistance properties which makes them best suited for applications with demanding mechanical stress requirements. The bending tests generated contradicting results between the two welds [26]. Results from ER 309L welding yielded superior bending resistance through the absence of cracks whereas ER NiCrMo-3 welds produced root-based cracks which extended to 86.3 mm and reached a minimum of 0.8 mm in length. The high mechanical strength observed in ER 309L welds demonstrates their advantage as building components for structures that depend on excellent bending resistance. The tensile testing produced important mechanical performance data. The tensile strength of ASTM 312 base metal reached 485 MPa but exhibited 170 MPa as its yield strength whereas API 5L Gr-B presented 415 MPa tensile strength and 240 MPa yield strength. Weld specimens connected with ER 309L failed at carbon steel base metal locations whereas ER NiCrMo-3 specimens failed at stainless steel base metal locations which demonstrates superior weld metal strength compared to base metal strength. The ultimate tensile strength values for ER 309L ranged between 448 MPa to 458 MPa while those of ER NiCrMo-3 were 534 MPa to 560 MPa demonstrating ER NiCrMo-3's superior strength potential however its vulnerability to bending-induced cracks is increased. The distinct failure mechanisms were verified through fractographic SEM examination. The welds made with ER 309L material

showed deeper but larger void formation while ER NiCrMo-3 welds exhibited denser void clusters within their structure which indicated better ductility. The deep voids present in ER NiCrMo-3 demonstrate its ability to deform plastically before failure which reflects better material toughness. SEM analysis demonstrates the necessity of choosing filler metals according to application needs because they determine both their hardness and ductility and corrosion resistance properties [27].

Conclusion

Research findings showed that ER 309L filler metal achieved superior weld quality through its low defect levels beyond those of ER NiCrMo-3 filler metal that contained limited porosity of 0.27 mm. Welds produced from ER 309L filler metal contained ferrite alongside acicular ferrite and pearlite structures which lead to increased weld hardness. The results of bending tests showed ER NiCrMo-3 welds developed cracks and ER 309L welds passed the test successfully which confirmed superior structural integrity in this weld material. ER NiCrMo-3 provided better ultimate tensile strength (550 MPa) than ER 309L (453 MPa) while the bending resistance was superior in ER 309L. Normal failure mode was verified through SEM which highlighted deeper voids in ER NiCrMo-3 samples because of their enhanced plastic deformation behavior. ER 309L provides the best solution when applications need hard welds with anti-structural failure properties while ER NiCrMo-3 functions best in demanding strength and corrosion-resistance applications.

Future Work

1. Welded joints undergo corrosion behavior assessments under aggressive environments to identify their lifespan potential.
2. The strategy focuses on studying different filler metals' effects on weld properties for better strength performance and environment-resistance while maintaining toughness of the materials.
3. Laboratory examinations of welded joint microstructures must analyze heat treatment methods to achieve best performance alongside reduced residual stress levels.

References

1. Kutelu BJ, Seidu SO, Eghabor GI, Ibitoye AI. Review of GTAW welding parameters. Journal of Minerals and Materials Characterization and Engineering. 2018;6(5):541-554. DOI:10.4236/jmmce.2018.65039.
2. Rigelsford J. Modern welding technology 5/e. Assembly Automation. 2003;23(3).
3. Low S, Steel A. Post-weld heat treatment of API 5L X70 high strength low alloy steel welds.
4. Kolawole FO, Kolawole SK, Agunsoye JO. Mitigation of corrosion problems in API 5L steel pipeline - A review. 2018;2508(8):2397-2410.
5. Topcu I, Karaman E. Cok Duvarh Karbon Nanotip Takviyeli Duzenli/Duzensiz Sekilli Ti-6Al-4V Kompozitlerin Asuma Davranışlarının İncelenmesi. Duzce Üniversitesi Bilim ve Teknoloji Dergisi. 2019;7(3):1249-1260.
6. Çınar O, Yaralı MC, Erdemir E, Çetiner BN, Mergen A, Gulluoğlu AN. The similar and dissimilar TIG welding of 316L and 321 austenitic stainless steels. ALKU Fen Bilimleri Dergisi. 2019;1(3):148-155.
7. Rathod DW, Pandey S, Singh PK, Kumar S. Microstructure-dependent fracture toughness (JIC) variations in dissimilar pipe welds for pressure vessel system of nuclear plants. Journal of Nuclear Materials. 2017;493:412-425.
8. Arora KS, Pandu SR, Shajan N, Pathak P, Shome M. Microstructure and impact toughness of reheated coarse grain heat affected zones of API X65 and API X80 linepipe steels. International Journal of Pressure Vessels and Piping. 2018;163:36-44.
9. ASTM A240/A240M. Standard specification for chromium and chromium-nickel stainless steel plate, sheet, and strip for pressure vessels and for general applications. ASTM International, West Conshohocken, PA. 2017.
10. Dutta J, Narendranath S. Estimation of cooling rate and its effect on temperature dependent properties in GTA welded high carbon steel joints. Welding Journal. 2014;10:149-155.
11. Lee WS, Tzeng FT, Lin CF. Mechanical properties of 304L stainless steel SMAW joints under dynamic impact loading. Journal of Materials Science. 2005;40:4839-4847.
12. Hajiannia I, Shamanian M, Kasiri M. Microstructure and mechanical properties of AISI 347 stainless steel/A335 low alloy steel dissimilar joint produced by gas tungsten arc welding. Materials & Design. 2013;50:566-573.
13. Phillips DH. Arc welding processes. In: Welding Engineering: An Introduction. First Edition. John Wiley & Sons; 2016. p. 4-73.
14. Seo DW, Jeon YB, Lim JK. Effect of electric weld current on spatter reduction in spot welding process. In: Key Engineering Materials. 2004;261:1623-1628.
15. Atma Raj MR, Joy Varghese VM. Determination of distortion developed during TIG welding of low carbon steel plate. International Journal of Engineering Research and General Science. 2014;2(5):756-767.
16. Tewari SP, Gupta A, Prakash J. Effect of welding parameters on the weldability of material. International Journal of Engineering Science and Technology. 2010;2(4):512-516.
17. Chuaiphan W, Srijaroenpramong L. Effect of welding speed on microstructures, mechanical properties, and corrosion behavior of GTA-welded AISI 201 stainless steel sheets. Journal of Materials Processing Technology. 2014;214(2):402-408.
18. Sayyar N, Shamanian M, Niroumand B. SC. Journal of Materials Processing Technology. 2018. DOI:10.1016/j.jmatprotec.2018.07.020.
19. Priceputu IL, Moisa B, Chiran A, Nicolescu G, Bacinschi Z. Delta ferrite influence in AISI 321 stainless steel welded tubes. 2011;6(6):87-90.
20. Cinar O, Yarali MC, Erdemir E, Çetiner BN. The similar and dissimilar TIG welding of 316L and 321 austenitic stainless steels. 2019;1(3):148-155.
21. Sharma S, Taiwade RV, Yadav A, Vashishtha H. Influence of fillers and welding processes on the microstructural evolution, mechanical properties, and corrosion behavior of dissimilar Hastelloy C-22/AISI 321 joints. Materials Research Express. 2019;6(9). DOI:10.1088/2053-1591/ab316b.
22. Saedi AH, Hajjari E, Sadrossadat SM. Microstructural

characterization and mechanical properties of TIG-welded API 5L X60 HSLA steel and AISI 310S stainless steel dissimilar joints. Metallurgical and Materials Transactions A. 2018. DOI:10.1007/s11661-018-4890-y.
23. Saffari H, Shamanian M, Bahrami A, Szpunar JA. Effects of ERNiCr-3 butter layer on the microstructure and mechanical properties of API 5L X65/AISI304 dissimilar joint. Journal of Manufacturing Processes. 2020;50:305-318. DOI:10.1016/j.jmapro.2019.12.028.
24. Asadollahi A, Bahrami A, Shamanian M. The effects of filler metal and butter layer on the microstructure and mechanical properties of API 5L X65/AISI 304L joint. Journal of Materials Research and Technology. 2023;23:4148-4166. DOI:10.1016/j.jmrt.2023.02.063.
25. Dak G, Pandey C. Microstructure anomaly during welding and its influence on the mechanical properties of dissimilar weldments of P92 martensitic steel and AISI 304L austenitic stainless steel. Journal of Manufacturing Processes. 2022;80:829-851. DOI:10.1016/j.jmapro.2022.06.048.
26. Zahraei SM, Dehmolaei R, Ashrafi A. The effect of heat input on microstructure and HAZ expansion in dissimilar joints between API 5L X80/DSS 2205 steels using thermal cycles. Revista de Metalurgia. 2022;58(1). DOI:10.3989/revmetalm.222.
27. Lee C, Chandel R, Seow H. Effect of welding parameters on the size of heat affected zone of submerged arc welding. Materials and Manufacturing Processes. 2000;15:649-666. DOI:10.1080/10426910008913011.